Tellus (2004), 56A, 287–295

TELLUS

Model predictions of coastal winds in a small scale

By HANNU SAVIJÄRVI*, *Division of Atmospheric Sciences, PO Box 64, Department of Physical Sciences, FIN-00014 University of Helsinki, Finland*

(Manuscript received 16 June 2003; in final form 16 February 2004)

ABSTRACT

Details of surface winds across a flat and non-curved coastline have been considered, mostly in the 1–10 km scale, by looking at some published observed cases and simulating with a high-resolution numerical model. Stability conditions were emphasized by having the land and sea at slightly different temperatures, but sea breeze conditions were excluded.

A warm surface generally enhances momentum transfer and wind speed, and reduces the cross-isobar angle. This transforms to rapid acceleration and downstream veering of offshore winds as they enter a warm, smooth sea. Cold sea, on the other hand, strongly inhibits vertical momentum transfer. This leads to offshore winds temporarily backing downstream off the coast, accelerating only slowly and even decreasing in speed in some cases. These observed facts were well simulated by the model.

Onshore flow on to cold land brought along rapid deceleration and strong inland backing of winds. The deceleration was weaker and more gradual over warm land with downstream veering instead. Smaller geostrophic wind speed accentuated these and all other stability effects as the wind shears then were weaker relative to the buoyancy effects (i.e. the absolute values of the local Richardson numbers were larger).

For large-scale winds along the shore with land on the right, the induced coastal convergence and rising motion appears only above about 100 m height in the cold sea simulations (typical of early summer). Below, there is divergence and hence relatively weak coastal wind. The case is the opposite for winds with land on the left (e.g. westerlies along a south coast): then the coastal surface winds are relatively strong along a cold sea. For a warm sea (typical of autumn) these low-level features disappear and coastal 10 m winds tend to be close to the geostrophic wind in speed and direction for all onshore directions.

1. Introduction

Details of surface winds near the coasts are important to many users (e.g. local duty weather forecasters, boat and ship operators, port authorities). Local winds also drive coastal currents and act on pollutant transport and dispersion near the coast. Routine wind observations are, however, usually made only on inland stations or on islands where the island itself is modifying the flow around it. Therefore, systematic observational information of wind at the sea near the coastline is scarcer than one might think. The case is handled in textbooks of general meteorology and of the boundary layer, but usually very briefly and superficially.

Wind is modified near the coasts on a small horizontal scale (1–10 km) mainly by the abrupt roughness change across the coastline, but stability may also vary rapidly if the land and sea surface temperatures differ. Mesoscale (∼10–100 km) phenomena, such as sea and land breezes and coastal low-level jets (e.g. Smedman et al., 1995) are also common. The detailed small-scale and mesoscale effects are not captured by numerical weather prediction models because of their relatively low horizontal resolution (grid length of 15–40 km). However, a high-resolution model (grid length of 1 km) should be able to produce these effects realistically.

This paper concentrates on the detailed systematic small-scale (1–10 km) effects in surface winds across a non-curved flat single coastline, caused by roughness and stability changes. First, three relevant observational studies (from the coasts of Denmark, Holland and eastern England) are reviewed. They are successfully simulated with a high-resolution two-dimensional model. Then, ‘typical’ 10-m wind speeds and directions across a flat coastline are presented from the model, for onshore and offshore 10 m s^{-1} geostrophic wind, the sea being either warm or cold. Finally, all geostrophic wind directions with speeds of 10 and 20 m s^{-1} are covered. The results are presented for convenience as for a southern coast, however they are independent of the direction of the coastline. Diurnal variation over land is reduced by either having an overcast cloud cover or keeping the land surface temperatures constant. Local topography effects (by, for example, islands, capes, inlets, curvature and sloping of the coastline) are excluded for simplicity; these may add their own signatures in reality.

*Corresponding author.
e-mail: hannu.savijarvi@helsinki.fi

The coastal mesoscale sea breezes, low-level jets and sea gulf effects in the 10–100 km scale will be considered in another paper. These flows, when present, provide the prevailing larger-scale winds near the coastline (instead of geostrophic wind), modified near the surface in the 1–10 km scale by the roughness and stability changes as described here.

The present experiments are extensions of Alestalo and Savijärvi (1985 hereafter AS), who studied roughness-implied effects in neutral flow across and along the coast. The model is here more advanced, the resolution is better, the important stability effects are realistically included and all wind directions are handled. The emphasis is on the 10-m wind details because AS covered the basic coastal convergence and the related vertical motion patterns quite well.

2. The model

We use the two-dimensional University of Helsinki (UH) high-resolution model, the sigma coordinate dynamical core of which originates from Alpert et al. (1982). The physical parametrizations include turbulence, advanced LW and SW radiation schemes, cloud physics and an interactive soil scheme. A large-scale pressure distribution in the form of constant geostrophic wind is given. The equations and details of the parametrizations can be found in the references below. The model's horizontal grid length is here 1 km. There are 132 grid points and 25 levels at the approximate altitudes of 2, 10, 30, . . . , 7000 m above the surface.

The turbulence scheme of the model is based on the Monin–Obukhov similarity treatment for the lowest layer and a mixing length approach aloft. This simple and robust first-order closure (in which the vertical diffusion coefficients are dependent on a squared mixing length, wind shear and stability) faired well, for example, in the comparison of Hess and Garratt (2002). The mixing lengths follow the Blackadar approach, the asymptotic mixing length being 150 m. The same stability functions $f(Ri)$ are used at all levels (local similarity; Sorbjan, 1986), which is natural as many model levels may be within the surface layer due to the high vertical resolution. *Ri* is the local bulk Richardson number evaluated from the predicted wind and temperature profiles. The present model version uses the standard Dyer–Businger forms for $f_{\mathrm{m}}(Ri)$ and $f_{\mathrm{h}}(Ri)$ in unstable conditions; in stable conditions a linear stability function $f_{\mathrm{m,h}}(Ri) = 1$–$5\ Ri$ is adopted with cut-off at 10% to preserve some turbulence.

The LW radiation scheme is basically the European Centre for Medium Range Weather Forecasts (ECMWF) six-band scheme, modified for more accuracy and stability in very high vertical resolution by Räisänen (1996); this is found important, for example, by Varghese et al. (2003). The SW scheme is a four-band two-stream GCM-type approach (Savijärvi et al., 1997). The force-restore soil scheme is from Savijärvi (1992).

The UH model has been used to study, for example, coastal convergence and sea/land breezes (AS; Neumann and Savijärvi, 1986; Savijärvi and Alestalo, 1988; Savijärvi, 1995), slope winds and nocturnal low-level jets (Savijärvi, 1991), the complex diurnal winds around Lake Tanganyika (Savijärvi, 1997), urban heat island circulations (Savijärvi, 1985; Savijärvi and Jin, 2001) and flow perturbations caused by heterogeneous landscape (Vihma and Savijärvi, 1991; Savijärvi and Amnell, 2001). There is also a version for planet Mars (e.g. Savijärvi and Siili, 1993; Savijärvi, 1999). In all these cases the model results have been close to the available time-mean and turbulence observations (for Mars, those from the Viking and Pathfinder landers) and have revealed the dynamics leading to the local flow perturbations induced by the variable lower boundary conditions.

Here the model parameters were set either to typical values or to the observed values, when available. The roughness length of momentum z_{om} is 0.1 mm over the sea and 50 cm over land, typical of sheltered seas and of the forest-patched scenery of Northern Europe, respectively. Over land, $z_{\mathrm{oh}} = z_{\mathrm{om}}$. The sea surface temperature (SST) is constant and the land surface temperature is either fixed or predicted, as indicated.

3. Offshore winds at the coastal zone

When air leaves the shore, both the near-surface wind speed and direction are likely to alter as the underlying surface becomes much smoother and usually either warmer or cooler than the air. The modifications take place in a few km scale over the sea so routine observations of it are rare. We describe here some special observations and augment these by model simulations.

3.1. Offshore wind speeds: the Öresund experiment

In the Öresund experiment, atmospheric dispersion processes and modifications in the wind across the 20 km wide Öresund strait between Denmark and Sweden were studied by having extra stations and ship observations in a line across the strait. Gryning et al. (1987) have reported the observed near-surface wind speeds during sunny days in June 1984, when the water (13 °C) was colder than the land and warm moderate winds blew from Sweden across the strait. Because the strait was so narrow, no sea breezes developed. The near-surface winds were found first to accelerate after the coastline. The average 10-m wind speed reached its maximum, 108% of that observed inland, 6 km off the coast. Subsequently the winds decelerated and at 20 km off the coast, winds were only 70–90% of that on the upwind (Swedish) coast. Thus, the roughness decrease initially dominated but development of a stable thermal internal boundary layer over the cool water then took over and inhibited vertical momentum transfer strongly. This was shown in Gryning et al. (1987) by experimenting with the Colorado State University (CSU) mesoscale model for one particular date, 5 June 1984.

We have simulated the same case using the UH model, giving the initial and other conditions as in Gryning et al. (1987) and

Table 1. The 10-m wind speed V and cross-isobar angle α across the coastline in the steady state of UH model simulation. Geostrophic wind 10 m s^{-1} is from land.

	Kilometres off coast											
	30	9	7	5	3	1	−1	−3	−5	−7	−9	−30
			(cold sea)						(land)			
Offshore winds, sea 3 °C colder than land												
V (m s^{-1})	6.6	5.5	5.4	5.2	5.0	4.4	3.7	3.4	3.3	3.3	3.2	3.1
α (°)	23.0	26.0	25.7	25.1	24.5	23.8	23.6	24.1	24.8	25.6	26.3	29.0
	Kilometres off coast											
	30	9	7	5	3	1	−1	−3	−5	−7	−9	−30
			(warm sea)						(land)			
Offshore winds, sea 3 °C warmer than land												
V (m s^{-1})	8.8	7.5	7.2	6.7	6.0	5.0	3.9	3.4	3.3	3.3	3.2	3.1
α (°)	11.0	19.5	20.2	20.8	21.6	22.4	23.3	24.4	25.3	26.2	26.9	29.0

Doran and Gryning (1987). Starting the integration at midnight, the 1200 local solar time (LT) clear-sky near-surface wind speed and air temperature profiles across the strait are similar to the ship observations and the CSU model profiles. Furthermore, the UH model's 10-m winds increase to 110% 6 km out at the sea and subsequently decrease to 85% 20 km downstream (on the Danish coast), as in the averaged observations. It thus appears that the UH model can simulate the changes in the wind speed quite well for offshore winds over cold water. The narrowness of the strait (20 km) may however strongly affect the winds. In Table 1 we therefore give the model values across a coastline on an open sea in two typical cases: warm sea and cold sea.

3.2. *Offshore wind directions: the Gorleston observations*

Even weak but systematic turning of coastal winds during offshore large-scale flow is important for sailing tactics and has been debated in that literature. The general belief is that an offshore near-surface wind always veers clockwise out at the sea as friction is much weaker over the smooth sea. Stability may, however, make things more complicated, as seen in the Öresund experiment.

Brettle and Smith (1999) have published results of a study of observed offshore westerly winds at Gorleston on the east coast of England. Sorting 10 yr of data by stability gave the result that the mean change in the observed wind direction at a (Smiths Knoll) lightship anchored some miles directly offshore, relative to the Gorleston winds at the coast, was veering of 7.5° on the 738 (unstable) occasions when the sea was warmer than the air by 3.3 °C or more, but anticlockwise backing of 5.5° on the 659 (stable) occasions when the sea was cooler than the air by 3.3 °C or more. Note that there was roughly the same amount of stable and unstable cases and that the overall average would indicate little or no turning.

3.3. *Offshore coastal winds: UH model results for open sea*

For offshore 10 m s^{-1} geostrophic wind, Table 1 gives the 'typical' 10-m wind speeds and the cross-isobar angles across the coastline at one nautical mile (2 km) intervals, calculated from the UH model wind component output. The sea is either 3 °C warmer or 3 °C cooler than the land surface, which is kept constant (at 15 °C). The model is run into a steady state (obtained in about 10 h) from an initial and inflow boundary state with air 15 °C at the surface and a lapse rate of 6.5 K km^{-1}. In other words, the flow approaching the coast has been adapted to its lower land boundary and its stability is the International Civil Aviation Organization (ICAO) average. Far inland, the 10-m wind is the same in both cases (speed 3.1 m s^{-1}, cross-isobar angle 29°) as can be expected because only the SST is varied between the two experiments.

The winds approaching a coldish sea accelerate moderately, but mainly after the coastline. A clockwise turning (veering) of the near-surface wind is noticed downstream a few kilometres before the coast in Table 1. In contrast, once at the cold sea the winds back relative to those at the coastal grid point, just as in the Gorleston observations for cold sea. A stable thermal internal boundary layer is forming downstream over the cold sea and the vertical momentum transfer is strongly inhibited because of that, just as in the Öresund experiment. Further out (>20 km) to the open sea the 10-m steady-state wind asymptotes to 6 m s^{-1}, 23°, so beyond 10 km off the coast (in the outer archipelago of the Finnish and Swedish waters) winds veer again. Seen from above, the horizontal streamlines of the flow form an S-shaped curve downstream from the coast. Well out at the cold sea, the offshore winds remain relatively weak with a largish cross-isobar angle for such a smooth surface. Warm advections (sometimes with advection fog forming over the cold sea) are typical cases of this type. A low-level jet may form downstream but it has little impact in the 1–10 km scale.

For sea warmer than land, offshore winds increase more rapidly downstream over the sea than in the cold sea case, according to Table 1. In contrast, wind speeds over land are practically the same in both cases. Winds start veering downstream already over land but in the case of a warm sea the veer continues off the coast, as in the Gorleston warm-sea observations. The 10-m wind far out at the open sea is in this case relatively strong, 8.8 m s^{-1}, 11°. Here the unstable stratification and the downstream-growing well-mixed layer enhance the wind speeds at the warm sea (via strong downward momentum transfer) and reduce the ageostrophic angle. Arctic cold air outbreaks out to non-frozen sea are extreme cases of this type.

If the temperature difference between air and sea is more than the 'typical' 3 °C chosen for the UH model simulations of Table 1 (and Table 3), the stability-dependent features, discussed above, become relatively even more accentuated.

4. Onshore winds at the coast

4.1. *Wind speed reduction over land: the Dutch observations*

When the air arrives from open sea toward land, the rough surface reduces wind speeds. An observational study of this was made in Holland (Kudryavtsev et al., 2000), by looking at the 10-m wind speeds at four Dutch inland weather stations, which were along a NW–SE line. A fifth station right at the shoreline gave the coastal benchmark. All onshore NW winds from the open North Sea sector (295–325°) from 11 August 1994 to 13 January 1995 were used and a stability index was recorded as well. The first station downstream from the coast, De Kooy, was 5 km inland; the next, Wijdenes, 42 km inland; then there was 20 km inland water (Lake Markermeer); Houtrib 63 km inland at the downstream lakeshore; and finally Lelystad 10 km downstream from the lake, 73 km downstream from the sea. Because of the autumn season, the sea was usually a few degrees warmer than land.

Table 2 gives the observed average wind speeds relative to that at the coastal station. Shown also are the values obtained from a UH model simulation, where the case is simulated by setting a 15 m s^{-1} geostrophic wind from an open sea 3 °C warmer than land, and calculating the reduction in the 10-m wind speeds from that at the coast in the distances similar to those of the observation sites. At 5 km inland (De Kooy) winds are about 70% of coastal winds and at 42 km from the coast (Wijdenes) they are 54% of that recorded at the seashore both in the model and in the observations. Winds then pick up over Lake Markermeer on the way to Houtrib. This process is underestimated in the UH model (the inland lake may have been smoother and warmer than the sea; sea values were used in the model because of a lack of information). 10 km further downstream over land, at Lelystad, onshore winds are however reduced again by about the same proportion in the observations and in the model.

Table 2. *The 10-m wind speed in per cent of that observed at the coastal station or in the model coastal grid point during onshore winds on the Dutch coast. Observed mean values are from Kudryavtsev et al. (2000).*

Station	De Kooy	Wijdenes	Houtrib	Lelystad
Observed	68.5%	54.0%	90.1%	62.5%
UH model	68.6%	54.3%	81.5%	56.6%

The model's inland reduction in wind speed appears to match the observations quite well, according to Table 2. The case is however complicated as the large and smooth inland lake is only 40 km from the ocean. Wind directions were not reported.

4.2. *Onshore coastal winds: UH model results for open sea*

Next, we present in Table 3 the 'typical' wind structure near the coast from the model experiments as in Table 1, but for 10 m s^{-1} geostrophic wind now directed from open sea on to flat land. The land is 3 °C colder or warmer than the sea. The inflowing air has been adapted to the sea surface (SST 15 °C, lapse rate 6.5 °C km^{-1}). Far out at sea (>20 km from coast) the steady-state 10-m wind is 7.2 m s^{-1}, 15° in these experiments, displaying the textbook sea values of 30% reduction in speed (relative to the geostrophic) and cross-isobar angle of 15°.

As these maritime winds approach cold land, the near-surface wind speed is reduced well ahead at sea and yet more over land while the winds begin to back already out at sea (Table 3). The backing is enhanced over the cold, stable land. Inland, the wind asymptotes to 2.5 m s^{-1}, 30°. Such weak winds and large cross-isobar angles are characteristic in inland observations of stable conditions, for instance during nighttime inversions.

In contrast, when onshore winds approach relatively warm land, they remain strong and steady right up to the shoreline in Table 3 with some backing between 10 and 30 km out at sea. Once over warm land, they start to reduce and veer. They stay stronger than in the stable case, being finally 4.2 m s^{-1}, 15° far downstream over the warm land. Note the small cross-isobar angle for a rough surface.

The warm land case is typical of summertime afternoon conditions. Perhaps because of that, it is also the only case usually considered in textbooks. As seen from Table 3, the wind behaves however quite differently in the cold land case.

5. Coastal winds: all wind directions

5.1. *Cold sea, strong winds*

The experiments for open sea are now repeated for all geostrophic wind directions relative to a south coast in 11.25°

Table 3. The 10-m wind speed V and cross-isobar angle α across the coastline in the steady state of UH model simulation. Geostrophic wind 10 m s^{-1} is from an open sea.

	Kilometres off coast											
	30	9	7	5	3	1	−1	−3	−5	−7	−9	−30
			(sea)						(cold land)			
Onshore winds, land 3 °C colder than sea												
V (m s^{-1})	7.2	6.9	6.8	6.5	6.0	4.9	3.6	2.9	2.7	2.6	2.5	2.5
α (°)	15.0	15.3	15.7	16.4	17.4	18.9	20.4	22.1	23.7	24.9	25.8	30.0
	Kilometres off coast											
	30	9	7	5	3	1	−1	−3	−5	−7	−9	−30
			(sea)						(warm land)			
Onshore winds, land 3 °C warmer than sea												
V (m s^{-1})	7.2	6.9	6.8	6.7	6.8	6.4	5.3	4.9	4.8	4.7	4.6	4.2
α (°)	15.0	20.0	20.4	20.7	20.3	19.0	16.9	15.0	14.0	13.2	12.6	15.0

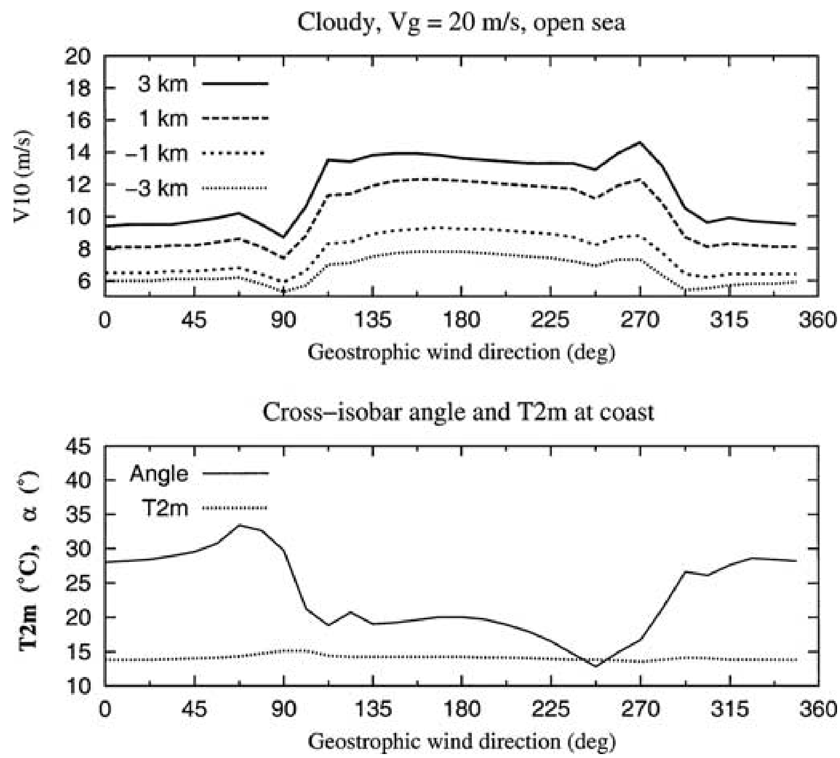

Fig 1. Top panel: the 10-m wind speed V10 (m s^{-1}) on a south-facing coast, 1 and 3 km over the sea and 1 and 3 km over land (−1, −3 km) as the function of the direction of strong (20 m s^{-1}) geostrophic wind. Onshore V_g is from 180°. Results are from UH model simulations for open, cold sea (SST 13 °C) in cloudy conditions at 1500 LT in June at 60°N. Bottom panel: the cross-isobar angle α (°) of the 10-m wind vector and the 2-m temperature T2m (°C), both in the coastal grid point of the model.

steps. A direction of 90° thus means easterly V_g along the coast (land on the right); 180° means onshore V_g. We introduce here a diurnal cycle by switching on all physics of the model. The integrations are started from midnight for typical parameter values of June in South Finland (60°N) so the sea is relatively cold; SST is 13 °C as in the Öresund observations. The diurnal variation is, however, damped by defining an overcast thick low cloud. As a result, the afternoon inland 2-m temperatures remain around 14–16 °C and no sea breezes appear. The results are shown for 1500 LT and the sea is open to the south. z_{om} is 0.1 mm over the sea and 50 cm over land.

A strongish constant geostrophic wind speed of 20 m s^{-1} is adopted first. The top panel of Fig. 1 displays the 10-m wind speeds (V10) from the model at 1500 LT as a function of direction of V_g. The bottom panel gives the respective cross-isobar angles and the 2-m temperature in the coastal grid point. V10 is given 1 and 3 km out at sea, and 1 and 3 km inland from the coast (−1 km, −3 km). Onshore V_g directions (180° ± 70°) are characterized in Fig. 1 by strongish wind speeds (V10 around 14 m s^{-1} 3 km out at sea) and smallish cross-isobar angles of 12–20°. Offshore V_g directions (0° ± 70°) are, on the other hand, characterized by weaker surface winds which accelerate rapidly out to sea, and by large coastal cross-isobaric angles (about 30°), as can be expected because the air enters the coast from over rough and not so warm land.

An interesting feature in Fig. 1 is the local minimum in V10 for easterly V_g, and maximum for westerly V_g. This is due to the fact that in the model's near-surface winds the frictionally-induced cross-isobar component is smaller over land than over the cold sea. Above about 100-m altitude, the situation is reversed. The same is true in the analytic Ekman–Taylor cross-isobar wind component profiles for realistic parameter values (cf. AS, their figure 2) so it is not just an artefact of the model. Therefore, for westerly geostrophic winds (i.e. land on the left of V_g), there must be near-surface convergence in the cross-isobar wind component across the coastline. This leads to strongish surface winds in the cold and very stable coastal zone.

These points are illustrated in Fig. 2, which shows the 1500 LT cross-sections of the wind components u, w from a model simulation with $(u_g, v_g) = (0, 20)$ m s^{-1} and land on the left (in grid points $x = 1$–59 km); the case corresponds to V_g from 270° in Fig. 1. V_g is into the figure so u (Fig. 2, top panel) is here the frictionally-induced cross-isobar component. Seaward from the coast (at $x = 60$–90 km) there is a shallow band of maximally negative u. Hence, cool maritime air converges to the coastal zone. In this very stable zone, conservation of mass leads into a shallow and small-scale band of rising motion (3 cm s^{-1}; Fig. 2, bottom panel) and strongish surface winds, which are concentrated near the coast (Fig. 1). The larger-scale main coastal divergence is seen in Fig. 2 in the form of sinking motion (w about -2 cm s^{-1}) at about 1-km altitude. This may tend to dissolve low clouds.

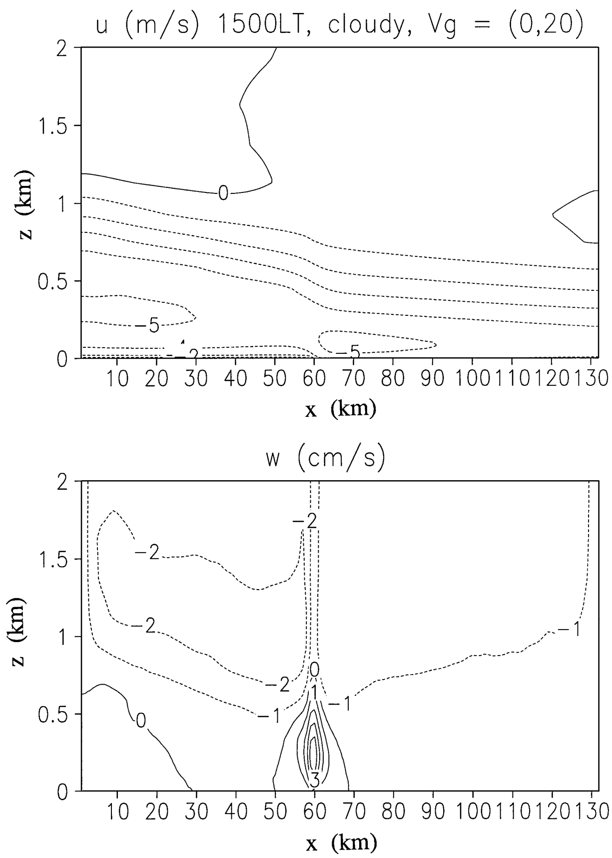

Fig 2. The 1500 LT wind components u (m s^{-1}, top panel) and w (cm s^{-1}, bottom panel) from the UH model simulation with V_g into the figure, $(u_g, v_g) = (0.0, 20.0)$ m s^{-1}. Land is on the left ($x = 1$–59 km), cold open sea is on the right ($x = 60$–132 km).

Exactly the opposite is true for easterly geostrophic winds (land on the right of V_g). Here, near-surface divergence across the coast leads into local sinking motion and the relatively weak 10-m coastal winds seen in Fig. 1 for V_g from 90°. However, the dominating larger-scale pattern of the main coastal convergence above 100 m and the associated maximum of rising motion at 500–700 m altitudes may induce bands of low cloud at the sea in this case. Such cloud bands are well illustrated in a satellite picture in Brettle and Smith (1999) in a case of northerly winds along the east coast of England. The position of the main cloud band matches with the position of the maximum rising motion, which is located about 20 km offshore, as shown in AS (their figure 6) for such a case.

These easily noticed bands of clouds over the sea and simplified reasoning about frictional differences have lead to the assumption that the coastal convergence reaches down to the surface and increases local coastal winds when land is on the right from the geostrophic wind. This is claimed in many weather guides for yachtsmen. Our model simulations predict just the opposite for a cold sea.

5.2. *Cold sea, moderate winds*

The above experiments have been repeated with more moderate geostrophic wind speed of 10 m s^{-1}, everything else remaining the same in the experiments. Figure 3 shows the result. The 10-m winds are now weaker than in Fig. 1. Interestingly, the roughness-change-induced difference in V10 between onshore and offshore winds is reduced. This is due to the fact that the stability effects are now enhanced (relative to Fig. 1) as the local Richardson numbers are larger in absolute value, due to the reduced vertical wind shear. The relative minima in V10 for easterly geostrophic winds and local maxima for westerly V_g discussed in Section 5.1 are accentuated for the same reason.

A new feature in Fig. 3 is the relatively strong V10 for geostrophic wind directions from 122° to 135° (ESE–SE). Noting the largish ageostrophic angles, we find that these surface winds tend, in fact, to blow along the shore (from the east), with a small component from the cold sea. The resulting shallow layer of cold, stable air at the coast leads to the increase in the cross-isobar angle and, in turn, to enhanced near-surface convergence and enhanced wind speeds.

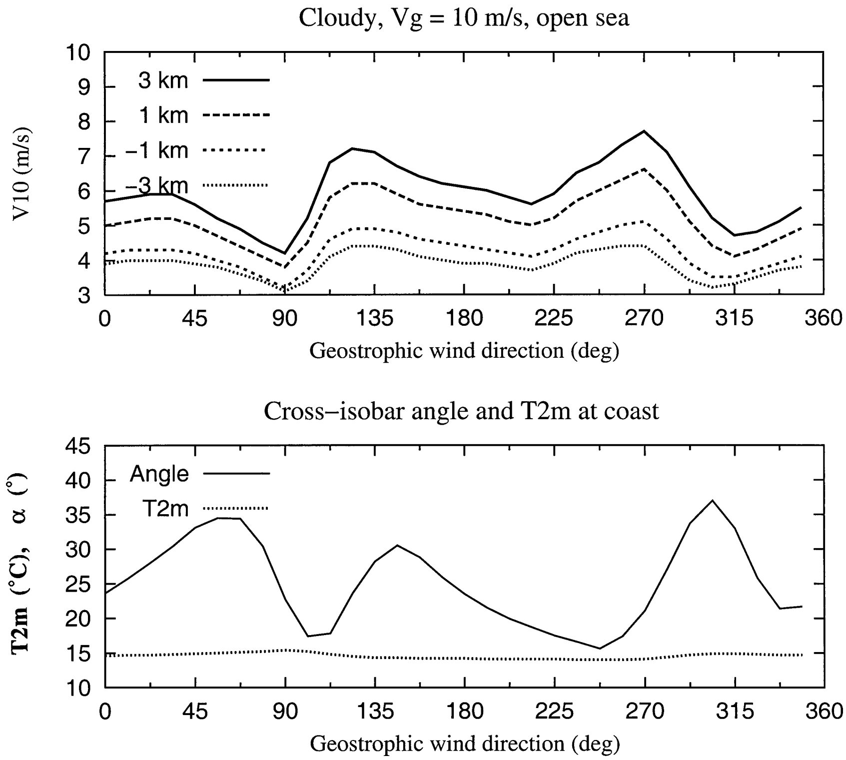

Fig 3. As for Fig. 1 but for $V_g = 10$ m s^{-1} (cold sea, moderate wind).

All the above features are enhanced even more if the sea is made relatively colder in the experiments. This is natural as they are due to the stability differences between land and sea.

5.3. *Warm sea*

The cloudy sky experiments with strong 20 m s^{-1} geostrophic wind from all directions are now repeated with the SST set to 18 °C. This is typical of late summer and autumn, and specifically in autumn baroclinic storms, where the large-scale winds are strong. The results are shown in Fig. 4. They may be compared with Fig. 1, the only difference being the 5 °C warmer sea surface, which makes the sea clearly warmer than the land even in the afternoon. Warm advection from the sea can be noticed in the 2-m temperatures at the coast, which are higher for all onshore wind directions in Fig. 4 than for offshore directions.

The warm sea enhances all coastal wind speeds, especially the onshore winds. The 10-m winds 3 km off the coast are 16–17 m s^{-1} in Fig. 4 for all V_g directions between 120° and 270° while the cross-isobar angles are small, around 10° or less. (Strong winds and small cross-isobar angles were also characteristic for the warm sea cases of Section 4.) The onshore 10-m winds are only 8 m s^{-1} 3 km inland so there is a strong gradient in wind speed across the coastline. The local wind speed minima for V_g of 90° and local maxima for V_g of 135° and 270° seen in Figs. 1 and 3 are absent in Fig. 4, because they were related to the cold sea and a stable coastal surface layer.

Figure 5 finally shows the warm sea integrations with more moderate V_g of 10 m s^{-1}. The wind speeds are stronger than in the respective cool sea case of Fig. 3. Onshore 10-m winds are here 80–90% of the geostrophic wind speed only 3 km into the sea, and the ageostrophic angles are small, between 5° and 10° at the coast. Offshore winds accelerate rapidly downstream to the warm sea, as in Table 1.

6. Summary

Details of surface winds across an open, flat, non-curved coast were considered by looking at some special observations, simulating them with a high-resolution model, and then making systematic simulations of typical conditions with the validated model. The purpose is to describe and explain the typical small-scale (1–10 km) features of the surface wind across the coast by using the high-resolution model as a laboratory, because these features are not detectable in the usual large-scale Numerical Weather Prediction (NWP) forecasts nor in the routine observational network. The simulations excluded sea breeze and low-level jet type phenomena by defining cloudy conditions. Hence, there is little diurnal variation over land and the main mechanism for wind changes is the roughness difference across the coast. Stability conditions near the coast were emphasized by having the land and sea at clearly different temperatures.

In the offshore flow cases, cold sea strongly inhibited vertical momentum transfer, which led to winds temporarily backing downstream just over the coastline, and even decreasing in speed

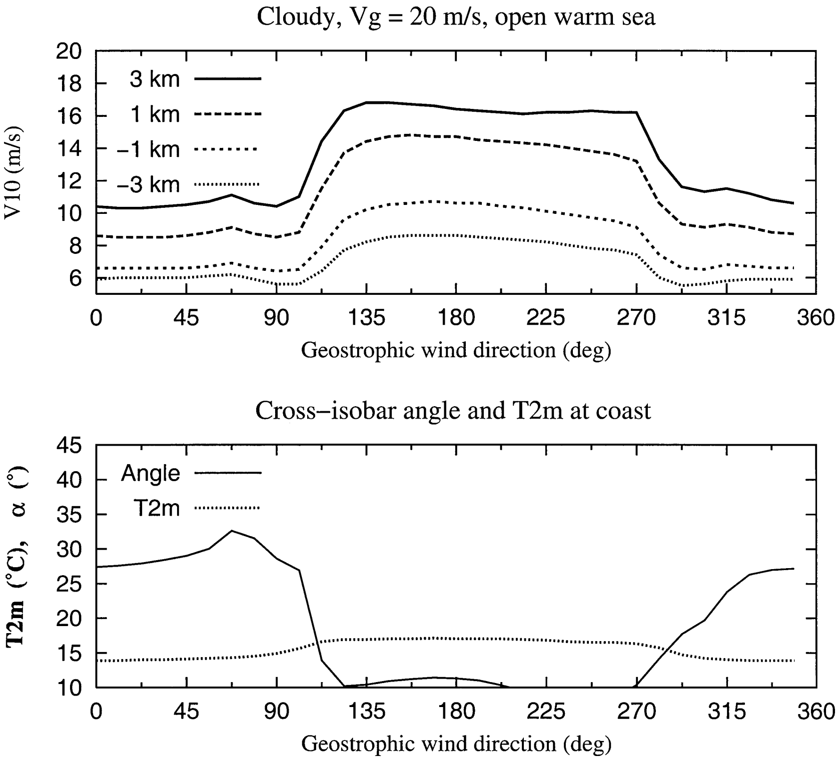

Fig 4. As for Fig. 1 but for SST = 18 °C (warm sea, strong wind).

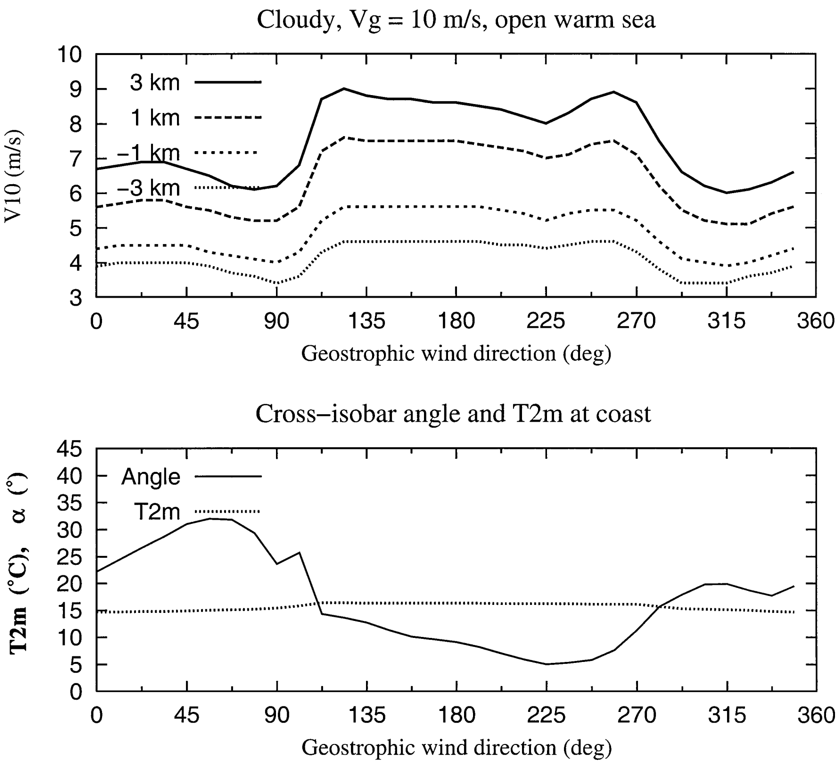

Fig 5. As for Fig. 4 but for $V_g = 10$ m s^{-1} (warm sea, moderate wind).

in some cases at sea. These observed facts were well simulated by the model. Warm sea, on the other hand, enhanced momentum transfer and hence enhanced the veer and acceleration of offshore winds off the coast.

During onshore flow, cold land brought about rapid deceleration and downstream backing of surface winds entering land, while these effects were weaker and more gradual when the land was warm compared to the sea. Weaker geostrophic winds accentuated these and all other stability effects as the wind shears then were weak compared to the buoyancy effects (i.e. the absolute values of the local Richardson numbers are large).

For large-scale winds along the shoreline with land on the right (easterly V_g along a south coast), coastal convergence appeared only above about 100-m height in the cold sea simulations. Below, there is divergence and hence relatively weak surface wind. For warm sea, this effect disappears or is much weaker. Exactly the opposite is true for winds with land on the left (westerly V_g along a south coast). Here, the near-surface coastal convergence together with strong stability caused by the cold sea (via its effects on the momentum transfer, cross-isobar angles, and cold advection) led to a band of relatively strong surface westerlies along the coast.

Largish cross-isobar angles over the cold sea also led to the tendency of relatively strong surface easterlies for moderate geostrophic winds from the south-east. For warm sea, this was no longer the case; instead, the 10-m winds 3 km off the coast were 80–90% of the geostrophic speed for all onshore wind directions and 60–70% for all offshore directions.

7. Acknowledgments

The work was supported by the Academy of Finland (contracts 167836 and 178457). The computations were made at the Center for Scientific Computing, Finland.

References

Alestalo, M. and Savijärvi, H. 1985. Mesoscale circulations in a hydrostatic model: Coastal convergence and orographic lifting. *Tellus*. **37A**, 156–162 (AS).

Alpert, P., Cohen, A., Doron, E. and Neumann, J. 1982. A model simulation of the summer circulation from the eastern Mediterranean past Lake Kinneret in the Jordan Valley. *Mon. Wea. Rev*. **110**, 994–1006.

Brettle, M. and Smith, B. 1999. *Weather to Sail*. Crowood Press, Marlborough, UK, 126 pp.

Doran, J. C. and Gryning, S.-E. 1987. Wind and temperature structure over a land–water–land area. *J. Clim. Appl. Meteorol*. **26**, 973–979.

Gryning, S.-E., Joffre, S. and Doran, J. C. 1987. The Öresund experiment – wind and temperature structure over a land–water–land area. *Bound. Layer Meteorol*. **41**, 309–318.

Hess, G. D. and Garratt, J. 2002. Evaluating models of the neutral barotropic planetary boundary layer using integral measures: Part II. Modelling observed conditions. *Bound. Layer Meteorol*. **104**, 359–369.

Kudryavtsev, V. N., Makin, V. K., Klein Tank, A. M. G. and Verkaik, J. W. 2000. A model of wind transformation over water–land surfaces. KNMI Scientific Report; WR-2000-01, KNMI, De Bilt, the Netherlands, 30 pp.

Neumann, J. and Savijärvi, H. 1986. The sea breeze on a steep coast. *Beitr. Phys. Atmos*. **59**, 375–389.

Räisänen, P. 1996. The effect of vertical resolution on clear-sky radiation calculations: tests with two schemes. *Tellus*. **48A**, 403–423.

Savijärvi, H. 1985. The sea breeze and urban heat island in a numerical model. *Geophysica*. **21**, 115–126.

Savijärvi, H. 1991. The U.S. Great Plains diurnal ABL variation and the nocturnal low-level jet. *Mon. Wea. Rev*. **119**, 833–840.

Savijärvi, H. 1992. On surface temperature and moisture prediction in atmospheric models. *Contr. Atmos. Phys*. **65**, 281–292.

Savijärvi, H. 1995. Sea breeze effects on large-scale atmospheric flow. *Contr. Atmos. Phys*. **68**, 335–344.

Savijärvi, H. 1997. Diurnal winds around Lake Tanganyika. *Q. J. R. Meteorol. Soc*. **123**, 901–918.

Savijärvi, H. 1999. A model study of the atmospheric boundary layer in the Mars Pathfinder lander conditions. *Q. J. R. Meteor. Soc*. **125**, 483–493.

Savijärvi, H. and Alestalo, M. 1988. The sea breeze over a lake or gulf as the function of the prevailing flow. *Beitr. Phys. Atmos*. **61**, 98–104.

Savijärvi, H. and Amnell, T. 2001. Horizontal variability in the wintertime boreal boundary layer: high resolution flight observations and numerical simulations. *Theor. Applied Clim*. **70**, 245–252.

Savijärvi, H. and Jin, L.-Y. 2001. Local winds in a valley city. *Bound.-Layer Meteorol*. **100**, 301–319.

Savijärvi, H. and Siili, T. 1993. The Martian slope winds and the nocturnal PBL jet. *J. Atmos. Sci*. **50**, 77–88.

Savijärvi, H., Arola, A. and Räisänen, P. 1997. Shortwave optical properties of precipitating waterclouds. *Q. J. R. Meteorol. Soc*. **123**, 883–899.

Smedman, A.-F., Bergström, H. and Högström, U. 1995. Spectra, variances and length scales in a marine stable boundary layer dominated by a low level jet. *Bound.-Layer Meteorol*. **76**, 211–232.

Sorbjan, Z. 1986. On similarity in the atmospheric boundary layer. *Bound.-Layer Meteorol*. **34**, 377–397.

Varghese, S., Murthy, A. S. V. and Narasimha, R. 2003. A fast, accurate method of computing near-surface longwave fluxes and cooling rates in the atmosphere. *J. Atmos. Sci*. **60**, 2869–2886.

Vihma, T. and Savijärvi, H. 1991. On the effective roughness length over heterogeneous terrain. *Q. J. R. Meteorol. Soc*. **117**, 399–408.